

## CHAPTER 64

### A NUMERICAL METHOD OF SOLITARY WAVE FORCES ACTING ON A LARGE VERTICAL CYLINDER

Takumi Ohyama <sup>1</sup>

#### ABSTRACT

Solitary wave forces acting on a large vertical cylinder are calculated using a time-stepping method which improves upon the conventional boundary element approaches. The effect of this improvement on the numerical solution is a more realistic solitary wave profile. Nonlinear effects on the solitary wave forces are investigated by comparing the numerical results with the first approximations given by Isaacson. The first approximation for overturning moment is underestimated remarkably when the incident wave height is relatively high.

#### 1. INTRODUCTION

In order to design coastal or offshore structures, accurate prediction of wave forces is necessary. In general, the incoming wave height considered during design is substantial, so that the nonlinear wave effects cannot be ignored and the linear potential theory may not predict realistic values of wave forces. Among various numerical studies applied to this problem, the methods of approach may be classified into two groups. One approach is based on a perturbation method. Using Stokes' wave theory, second approximations for wave forces acting on a large vertical cylinder have been recently introduced by many researchers. For example, Hunt and Buddour (1981) gave the solution for deep water, and Eatock Taylor and Hung (1987) attempted to derive the definite solution for arbitrary water depth. However, this type of approach cannot be directly extended to higher-order expansions because of difficulties in the treatment of the free surface condition and the nonlinear radiation condition.

---

<sup>1</sup>Institute of Technology, SHIMIZU CORPORATION, Etchujima 3-4-17, Koto-ku, Tokyo 135, JAPAN

The other approach is a time-stepping method in which the boundary integral equations based on Green's theorem are solved at successive time steps. In this approach, the complete boundary value problem of velocity potential is considered without using the assumption of weak nonlinearity. For example, Isaacson (1982) applied this boundary integral equation method to the problem of nonlinear wave scattering around three-dimensional bodies. A similar method was proposed by Nakayama and Washizu (1981) for two-dimensional sloshing problems. However, the potential values on free surfaces were not estimated accurately in the time-stepping procedure of these conventional methods.

This paper studies interactions between a solitary wave and a large vertical cylinder using a newly developed numerical method. The proposed technique treats the interaction as a three-dimensional transient problem, and it improves the time-stepping procedure of the conventional boundary element methods. The effect of the improvement on the numerical solution is investigated by fundamental examinations. Nonlinear effects on wave forces exerted by a solitary wave on a circular cylinder are discussed by comparing the numerical results with first approximations given by Isaacson (1983). The results obtained from this study may be applicable to the design of coastal structures in shallow water.

## 2. THEORETICAL FORMULATION

### 2.1 Boundary Integral Equations

Consider a three-dimensional fluid region  $\Omega$  as shown in Fig. 1. The region is enclosed by the free surface  $S_F$ , the body wetted surface  $S_V$ , the wave generating boundary  $S_C$ , the wall boundaries  $S_{W1}$ ,  $S_{W2}$ ,  $S_{W3}$ , and the seabed  $S_B$ . The boundaries,  $S_C$ ,  $S_{W1}$ ,  $S_{W2}$ , and  $S_{W3}$ , are located sufficiently far from the body so that the diffracted waves will not reach these boundaries during the duration of computation. The fluid is assumed to be incompressible, inviscid and irrotational, so that the fluid motion can be described by a velocity potential  $\phi$ . The velocity potential can be given as the solution satisfying the following governing equation and the associated boundary conditions:

$$\nabla^2 \phi = 0 \quad (\text{in } \Omega), \quad (1)$$

$$\partial \phi / \partial n = 0 \quad (\text{on } S_B, S_{W1}, S_{W2}, S_{W3}), \quad (2)$$

$$\partial \phi / \partial n = 0 \quad (\text{on } S_V), \quad (3)$$

$$\partial \phi / \partial n = -\partial \phi / \partial x = -U(z, t) \quad (\text{on } S_C), \quad (4)$$

$$\partial \phi / \partial n = n_z (\partial \eta / \partial t) \quad (\text{on } S_F), \quad (5)$$

$$\partial \phi / \partial t + (1/2)(\nabla \phi)^2 + g\eta = 0 \quad (\text{on } S_F), \quad (6)$$

in which  $n$  and  $n_z$  are the direction and the  $z$ -component of outward unit normal vector  $n$  defined on the boundary surfaces, respectively, and  $\eta$  is the free surface elevation above the still water level.  $U$  in Eq. (4) denotes the water particle velocity in the  $x$ -direction of the solitary wave given by the analytical solutions. Equation (1) corresponds to the continuity equation of the fluid motion. Equations (2) and (3) relate to the impermeable conditions on the seabed and the walls and the body surface, respectively. In generating waves, the still-water condition is applied as an initial condition, and the kinematic condition as indicated in Eq. (4) is imposed on  $S_C$ . Equations (5) and (6) represent the kinematic and the dynamic conditions on  $S_F$ , which are considered to be nonlinear.

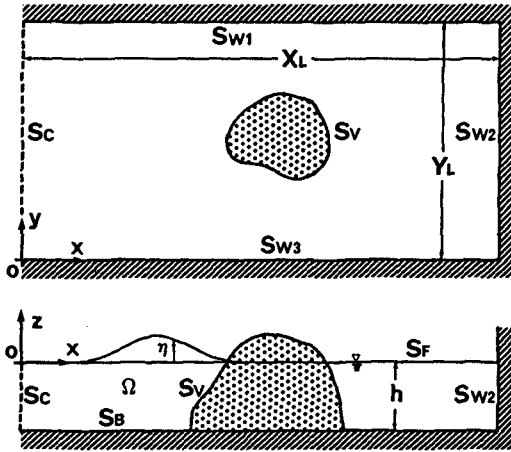


Fig. 1 Coordinate system.

Applying the second form of Green's theorem over the closed surface  $S$  containing the fluid region  $\Omega$ , a boundary integral equation is introduced in which the boundary values of the potential  $\phi$  are related to those of the normal derivative  $\partial\phi/\partial n$ . The potential  $\phi(P)$  at the point  $P(x_P, y_P, z_P)$  which lies on  $S$  is expressed as

$$\phi(P) = -\frac{1}{\alpha(P)} \int_S \left\{ \phi(Q) \frac{\partial G}{\partial n}(P, Q) - \frac{\partial \phi}{\partial n}(Q) G(P, Q) \right\} ds, \tag{7}$$

where  $Q(x_Q, y_Q, z_Q)$  is a point lying on  $S$  where the integration is performed and  $G$  represents a Green function.  $\alpha(P)$  denotes a coefficient calculated by

$$\alpha(P) = - \int_{S_F \cup S_C \cup S_{W3} \cup S_V} \frac{\partial G}{\partial n} ds. \tag{8}$$

The Green function involved in Eq. (7) is chosen to account for the symmetry about the boundaries,  $S_B, S_{W1}$ , and  $S_{W2}$ , such that

$$G(P, Q) = \frac{1}{r_0} + \sum_{n=1}^7 \frac{1}{r_n}, \tag{9}$$

$$\left. \begin{aligned}
 r_0 &= \sqrt{(C_x)^2 + (C_y)^2 + (C_z)^2}, & r_1 &= \sqrt{(C_x)^2 + (C_y)^2 + (D_z)^2}, \\
 r_2 &= \sqrt{(C_x)^2 + (D_y)^2 + (C_z)^2}, & r_3 &= \sqrt{(C_x)^2 + (D_y)^2 + (D_z)^2}, \\
 r_4 &= \sqrt{(D_x)^2 + (C_y)^2 + (C_z)^2}, & r_5 &= \sqrt{(D_x)^2 + (C_y)^2 + (D_z)^2}, \\
 r_6 &= \sqrt{(D_x)^2 + (D_y)^2 + (C_z)^2}, & r_7 &= \sqrt{(D_x)^2 + (D_y)^2 + (D_z)^2}, \\
 C_x &= x_P - x_Q, & D_x &= x_P + x_Q - 2X_L, \\
 C_y &= y_P - y_Q, & D_y &= y_P + y_Q - 2Y_L, \\
 C_z &= z_P - z_Q, & D_z &= z_P + z_Q + 2h,
 \end{aligned} \right\} \quad (10)$$

in which  $X_L$  and  $Y_L$  are the length and the width of the fluid region, respectively, as shown in Fig. 1. This Green function satisfies  $\partial G/\partial n = 0$  on  $S_{W1}$ ,  $S_{W2}$  and  $S_B$ , so that the integrals over these boundaries can be excluded from Eq. (7). Substituting Eqs. (2), (3), (4) and (5) into Eq. (7), the following integral equation is introduced:

$$\phi(P) = -\frac{1}{\alpha(P)} \left\{ \int_{S_F \cup S_C \cup S_{W3} \cup S_V} \phi \frac{\partial G}{\partial n} ds - \int_{S_F} G n_z \frac{\partial \eta}{\partial t} ds + \int_{S_C} G U ds \right\}, \quad (11)$$

The dynamic condition on  $S_F$  can be transformed into another integral equation by applying the method of weighted residuals. Substituting Eq. (5) into Eq. (6) and integrating it over  $S_F$  after multiplying both sides by a weighting function  $\omega$ , the following integral equation can be obtained:

$$\int_{S_F} \omega \left[ \frac{\partial \phi}{\partial t} + \frac{1}{2} \left\{ n_z^2 \left( \frac{\partial \eta}{\partial t} \right)^2 + \left( \frac{\partial \phi}{\partial X} \right)^2 + \left( \frac{\partial \phi}{\partial Y} \right)^2 \right\} + g \eta \right] ds = 0, \quad (12)$$

where  $(X, Y)$  is a local coordinate system on the surface plain normal to the vector  $n$  as shown in Fig. 2.

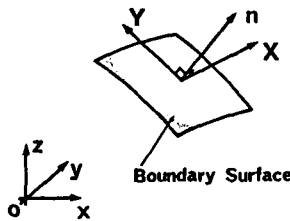


Fig. 2 Local coordinates on the free surface.

### 2.2 Spatial Discretization of Integral Equations

The boundary surfaces,  $S_F$ ,  $S_C$ ,  $S_{W3}$ , and  $S_V$ , are discretized into finite numbers of triangle elements. The local coordinate system  $(X, Y)$  is defined as indicated in Fig.3 over each element. In this figure,  $j1, j2, j3$  are nodal point numbers comprising the  $J$ -th element, and  $R$  denotes a point on the element. Representing the variables of  $\phi, \eta, U$  and  $\omega$  as  $\Gamma$ , the values of  $\Gamma$  and  $\partial\Gamma/\partial t$  on  $R$  can be written as

$$\Gamma = N_J^T \mathbf{\Gamma}_J, \quad \mathbf{\Gamma}_J^T = \{\Gamma_{j1}, \Gamma_{j2}, \Gamma_{j3}\}, \quad (13)$$

$$\frac{\partial \Gamma}{\partial t} = N_J^T (\Gamma_t)_J, \quad (\Gamma_t)_J^T = \left\{ \left( \frac{\partial \Gamma}{\partial t} \right)_{j1}, \left( \frac{\partial \Gamma}{\partial t} \right)_{j2}, \left( \frac{\partial \Gamma}{\partial t} \right)_{j3} \right\}, \quad (14)$$

in which  $N_J$  represents interpolation function vector. If linear distributions of  $\Gamma$  and  $\partial \Gamma / \partial t$  over the element are assumed,  $N_J$  can be expressed as

$$N_J^T = (1/S_J) \{S_{j1}, S_{j2}, S_{j3}\}, \quad (15)$$

where  $S_{j1}$ ,  $S_{j2}$  and  $S_{j3}$  are defined in Fig. 3 and  $S_J$  is the area of the  $J$ -th element ( $= S_{j1} + S_{j2} + S_{j3}$ ).

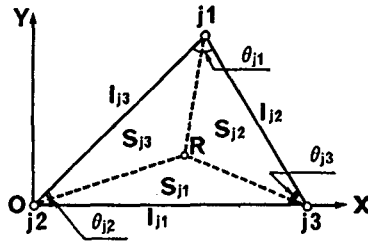


Fig. 3 Definition sketch in the  $J$ -th element.

Using the expressions of Eqs. (13) and (14), the integral equation (11) is transformed into

$$\alpha_i \phi_i + \sum_{J=1}^M A_{iJ}^T \phi_J - \sum_{J=1}^{M_F} (n_z)_J B_{iJ}^T (\eta_t)_J + \sum_{J=M_F+1}^{M_F+M_C} B_{iJ}^T U_J = 0 \quad (i = 1, 2, \dots, N), \quad (16)$$

$$A_{iJ} = \int_{S_J} N_J \frac{\partial G}{\partial n} ds, \quad B_{iJ} = \int_{S_J} N_J G ds, \quad (17)$$

in which  $M$  and  $N$  are the total numbers of triangle elements and the nodal points, respectively.  $M$  is made up of  $M_F$  elements over  $S_F$ ,  $M_C$  elements over  $S_C$ ,  $M_V$  elements over  $S_V$ , and  $M_W$  elements over  $S_{W3}$ . The surfaces are treated in order  $S_F$ ,  $S_C$ ,  $S_V$  and  $S_{W3}$  as  $J$  increases from 1 to  $M$ . The vectors,  $A_{iJ}$  and  $B_{iJ}$  can be calculated numerically, even when  $i$  coincides with  $j1$  or  $j2$  or  $j3$ . Numerical integrals over all the elements, however, may require time-consuming computational efforts. Therefore, the calculations of  $A_{iJ}$  and  $B_{iJ}$  are simplified by assuming those values to be constant over the  $J$ -th element, when  $i \neq j1$  nor  $j2$  nor  $j3$ . Thus

$$A_{iJ} \simeq \frac{S_J}{3} \left( \frac{\partial G}{\partial n} \right)_{iJ} \mathbf{E}, \quad B_{iJ} \simeq \frac{S_J}{3} G_{iJ} \mathbf{E} \quad (i \neq j1, j2, j3), \quad (18)$$

$$\mathbf{E}^T = (1, 1, 1), \quad (19)$$

where  $(\partial G/\partial n)_{iJ}$  and  $G_{iJ}$  are the corresponding values at the center of gravity in the  $J$ -th element.

Substituting Eqs. (13) and (14) into Eq. (12), we obtain

$$\sum_{J=1}^{M_F} \left[ \int_{S_J} N_J N_J^T ds (\phi_t)_{iJ} + \frac{(n_z)_J^2}{2} \int_{S_J} N_J N_J^T (\eta_t)_{iJ} N_J^T ds (\eta_t)_{iJ} + \frac{1}{2} \{ (\phi_X)^2 + (\phi_Y)^2 \}_J \int_{S_J} N_J ds + g \int_{S_J} N_J N_J^T ds \eta_{iJ} \right] = 0. \quad (20)$$

The velocity squared on the surface plain,  $\{ (\phi_X)^2 + (\phi_Y)^2 \}_J$ , is assumed to be constant over the  $J$ -th element. That is,

$$\begin{aligned} \{ (\phi_X)^2 + (\phi_Y)^2 \}_J &= \frac{1}{4S_J^2} \{ (l_{j1}\phi_{j1})^2 + (l_{j2}\phi_{j2})^2 + (l_{j3}\phi_{j3})^2 \} \\ &\quad - \frac{1}{S_J} \left\{ \frac{\phi_{j1}\phi_{j2}}{\tan \theta_{j3}} + \frac{\phi_{j2}\phi_{j3}}{\tan \theta_{j1}} + \frac{\phi_{j3}\phi_{j1}}{\tan \theta_{j2}} \right\}. \end{aligned} \quad (21)$$

The integrals involved in Eq. (20) can be calculated analytically and may be transformed into the form

$$\sum_{j=1}^{N_F} \gamma_j \omega_j = 0, \quad (22)$$

where  $N_F$  is the number of the nodal points on the free surface.  $\gamma_j$  involves  $\phi_j$ ,  $(\partial\phi/\partial t)_j$ ,  $\eta_j$ ,  $(\partial\eta/\partial t)_j$  ( $j = 1, 2, \dots, N_F$ ) as unknown variables (see Ohyama, 1989 b). The arbitrariness of the weighting function  $\omega$  leads to the equation

$$\gamma_j = 0 \quad (j = 1, 2, \dots, N_F). \quad (23)$$

### 2.3 Time-Stepping Procedure

The discretized equations (16) and (23) are solved simultaneously for successive time steps to estimate the wave motion transition. The surface elevation and the velocity potential at the  $n$ -th time step,  $\eta^{(n)}$  and  $\phi^{(n)}$ , are given as

$$\eta^{(n)} = \eta^{(n-1)} + \Delta\eta^{(n)}, \quad \phi^{(n)} = \phi^{(n-1)} + \Delta\phi^{(n)}, \quad (24)$$

in which  $\Delta\eta^{(n)}$  and  $\Delta\phi^{(n)}$  represent the increments of  $\eta$  and  $\phi$  during the time increment  $\Delta t$ , respectively. Using Taylor expansions around the corresponding values at the  $(n-1)$ -th time step and neglecting the higher order terms with respect to  $\Delta t$ ,  $(\partial\eta/\partial t)^{(n)}$  and  $(\partial\phi/\partial t)^{(n)}$  can be expressed as

$$\left( \frac{\partial\eta}{\partial t} \right)^{(n)} = \frac{2\Delta\eta^{(n)}}{\Delta t} - \left( \frac{\partial\eta}{\partial t} \right)^{(n-1)}, \quad (25)$$

$$\begin{aligned} \left( \frac{\partial\phi}{\partial t} \right)^{(n)} &= \frac{2\Delta\phi^{(n)}}{\Delta t} - \left( \frac{\partial\phi}{\partial t} \right)^{(n-1)} - \frac{2\Delta\eta^{(n)}}{\Delta t} \left( \frac{\partial\phi}{\partial z} \right)^{(n-1)} \\ - \Delta t \left( \frac{\partial\eta}{\partial t} \right)^{(n-1)} \left( \frac{\partial^2\phi}{\partial z\partial t} \right)^{(n-1)} &+ \left( \frac{\partial\eta}{\partial t} \right)^{(n-1)} \left( \frac{\partial^2\phi}{\partial z^2} \right)^{(n-1)} \quad (\text{on } S_F). \end{aligned} \quad (26)$$

It should be noted that Taylor expansions, with respect not only to time but also to spatial displacement, must be applied to the estimation of the potential values on  $S_F$ . The last three nonlinear terms on the right-hand side of Eq. (26) correspond to the change in location of the nodal point on  $S_F$ . In the method proposed by Nakayama and Washizu (1981) for two-dimensional sloshing problems, only the expansions with respect to time were considered, so that these nonlinear terms were entirely neglected. Isaacson (1982) also omitted the effect of spatial displacement from the time-stepping procedure. However, the partial effects were taken into account in a recent paper (Isaacson and Zuo, 1989).

Substituting Eqs. (24), (25) and (26) into Eqs. (16) and (23), the linear algebraic equations for  $\Delta\phi_j^{(n)}$  ( $j = 1, 2, \dots, N$ ) and  $\Delta\eta_j^{(n)}$  ( $j = 1, 2, \dots, N_F$ ) can be obtained. The quantities associated with the boundary surface profile,  $S_J$ ,  $(n_x)_J$ ,  $A_{iJ}$ ,  $B_{iJ}$ , and so on, are unknown when solving the equations at each time step, since  $\Delta\eta_j^{(n)}$  are involved in the equations as unknown variables. Thus, in order to obtain the successful solutions associated with the corresponding free surface profile, the iteration procedure is applied using the surface profile at the previous time step as the initial profile (see Ohyama, 1985). It usually takes two or three iterations to obtain the convergence.

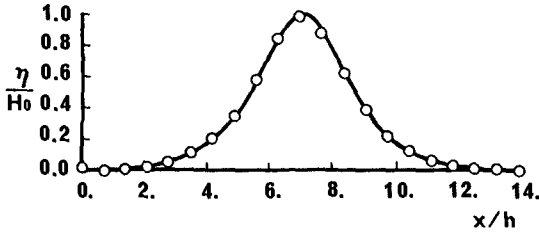
### 3. ACCURACY AND FUNDAMENTAL EXAMINATIONS

Fundamental examinations were carried out to confirm the validity of the proposed method. Solitary waves with various wave heights,  $H_0$ , were generated numerically in a three-dimensional wave channel with a constant depth  $h$  and a constant width  $Y_L$ . In the computations, the still water condition ( $\phi = \eta = 0$ ) inside the region was considered as an initial condition, and the third approximation given by Fenton (1972) was applied to the velocity  $U$  imposed on  $S_C$ . The numerical results were compared with the third approximation in terms of the generated wave profile and the hydrodynamic pressure. Once the velocity potential  $\phi$  is given at successive time steps, the pressure  $p$  can be obtained from the Bernoulli equation

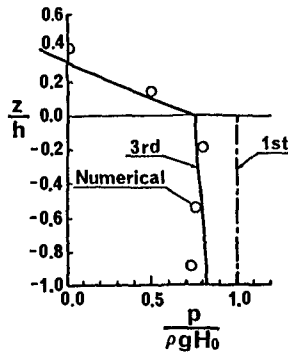
$$p = -\rho \left\{ (\partial\phi/\partial t) + (1/2)(\nabla\phi)^2 + gz \right\}, \quad (27)$$

where  $\rho$  is the fluid density. The results for the case of  $H_0/h = 0.4$  are shown in Figs. 4 (a) and 4 (b) together with the corresponding approximations. In this calculation,  $X_L/h$  and  $Y_L/h$  were fixed at 14.0 and 2.1, respectively. According to the results of the previous study for a two-dimensional numerical model (Ohyama, 1989 a), the maximum horizontal distance between the neighboring nodal points on  $S_F$ ,  $\Delta l$ , and the time increment  $\Delta t$  were varied with  $H_0/h$ . In the case of  $H_0/h = 0.4$ ,  $\Delta l/h$  and  $\Delta t\sqrt{g/h}$  were set at 0.7 and 0.4, respectively. As shown in Figs. 4 (a) and 4 (b), the agreements between the numerical result and the third approximation

are fairly good, whereas the first approximation predicts a remarkably larger value for hydrodynamic pressure under the still water level. It may indicate that the proposed method can well predict the wave motion and the induced force even in the case of a relatively high wave height.



(a) Generated solitary wave profile ( $y/h = 0$ )



(b) Distribution of hydrodynamic pressure under the wave crest

Fig. 4 Comparisons with the corresponding approximation for  $H_0/h = 0.4$  ;  
 ○, numerical result; —, third approximation; ---, first approximation.

Additional examinations were performed to ascertain the effect on the numerical solutions of taking into account the nonlinear terms in Eq. (26). Figure 5 shows the numerical result of the generated wave profile with  $H_0/h = 0.4$ , together with the third approximation. The results calculated by the proposed method and those by the conventional method, in which the nonlinear terms in Eq. (26) are neglected, are denoted by circles and triangles, respectively. It should be noted that the proposed method can eliminate the numerical error accumulation which occurs in the conventional analysis.

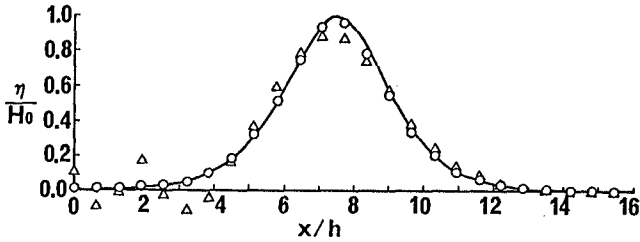


Fig. 5 Generated solitary wave profile with  $H_0/h = 0.4$  ;  
 ○, numerical result taking into account the nonlinear terms in Eq. (26);  
 △, numerical result neglecting the nonlinear terms in Eq. (26);  
 —, third approximation given by Fenton, 1972.

#### 4. NONLINEAR EFFECTS ON SOLITARY WAVE FORCES

First approximation for the solitary wave diffraction around a circular cylinder was already given in closed form by Isaacson (1982). According to this approximation, a maximum force coefficient,  $C_F$ , and a maximum overturning moment coefficient,  $C_M$ , are conveniently described by the single number  $(a/h)\sqrt{H_0/h}$ , in which  $C_F$  and  $C_M$  are defined as

$$C_F \equiv \frac{F_{max}}{\rho g H_0 a h}, \quad C_M \equiv \frac{M_{max}}{\rho g H_0 a h^2}, \quad (28)$$

where  $F_{max}$  and  $M_{max}$  denote the maximum horizontal force and the maximum overturning moment, respectively, and  $a$  is the cylinder radius. However, the first approximations were introduced on the assumption of a small wave height. Thus, nonlinear effects on solitary wave forces acting on the cylinder may be discussed by comparing the numerical result with the first approximation.

Figure 6 shows the free surface elevation computed by the proposed method in the case of  $(a/h)\sqrt{H_0/h} = 2.0$  and  $H_0/h = 0.4$ , when the horizontal force acting on the cylinder is at the maximum. Only the half side of the fluid region was considered in the calculation because of the symmetry of the circular cylinder. In the case indicated in Fig. 6, the surfaces  $S_F$ ,  $S_C$ ,  $S_V$  and  $S_{W3}$  were discretized into 846, 120, 112, and 176 elements, respectively, and the total number of the nodal points was 680.

The corresponding numerical results of the temporal variations of the horizontal force  $F_x$  and the overturning moment  $M_y$  are indicated in Figs. 7 (a) and 7 (b), together with the first approximation. The abscissa in these figures represents nondimensional time, where  $t'$  denotes time measured from the instant when the crest of the incident wave passes the center of the cylinder. The calculation was carried out for  $H_0/h$  being 0.1 and 0.4. In the case of  $H_0/h = 0.1$ , the agreements between the numerical result and the first approximation are fairly good for both the horizon-

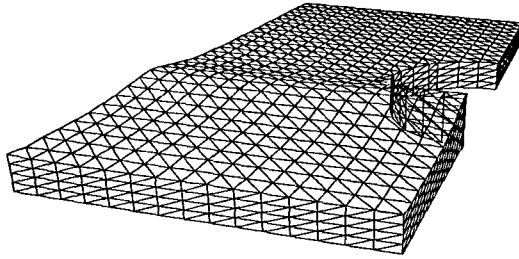
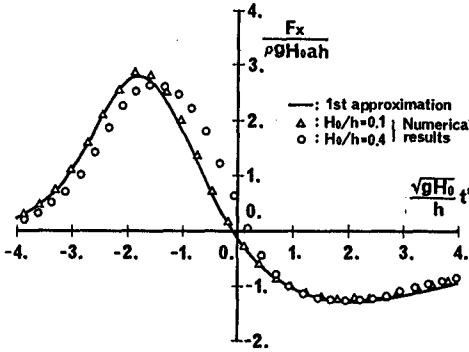


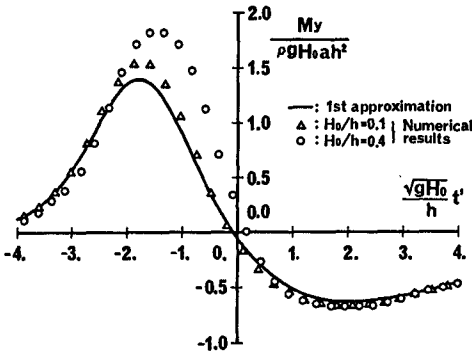
Fig. 6 Free surface elevation with  $(a/h)\sqrt{H_0/h} = 2.0$  and  $H_0/h = 0.4$ .

tal force and the overturning moment. For  $H_0/h = 0.4$ , however, the prediction of the maximum overturning moment is remarkably larger than the first approximation, whereas the difference in the maximum horizontal force may not be notable. The reason why the prediction of the overturning moment for  $H_0/h = 0.4$  is larger than the first approximation may be explained by the following facts. First, **Figure 8** shows the distribution of hydrodynamic pressure in a horizontal cross section when the horizontal force is at the maximum. For  $H_0/h = 0.4$ , the pressure over the cylinder surface is found to be smaller than the value predicted by the approximation. This characteristic is the same as the progressive solitary wave, as indicated in **Fig. 4 (b)**. Second, the proposed method takes into account the pressure distribution above the still water level, whereas it is neglected in the first approximation. These two facts have contrary effects on the prediction of the horizontal force, so that the numerical results of the horizontal force may differ slightly from the approximation, even for the case of  $H_0/h = 0.4$ . Furthermore, the second fact explains that the point of the resultant force shifts upward as the incident wave height increases. Thus, compared to the approximation, the proposed method predicts a larger value for the overturning moment.

**Figures 9 (a)** and **9 (b)** show the variations of  $C_F$  and  $C_M$  with  $(a/h)\sqrt{H_0/h}$ , respectively. When the value of  $(a/h)\sqrt{H_0/h}$  is small, the differences between the numerical result and the first approximation are not significant, even for the overturning moment. As this parameter  $(a/h)\sqrt{H_0/h}$  becomes larger, however, the approximation predicts a much smaller magnitude of overturning moment. The prediction obtained from the numerical calculation shows a 40% larger value than the approximation for  $(a/h)\sqrt{H_0/h} = 3.0$  and  $H_0/h = 0.4$ .



(a) horizontal force



(b) overturning moment

Fig. 7 Temporal variations of horizontal force and overturning moment for  $(a/h)\sqrt{H_0/h} = 2.0$ .

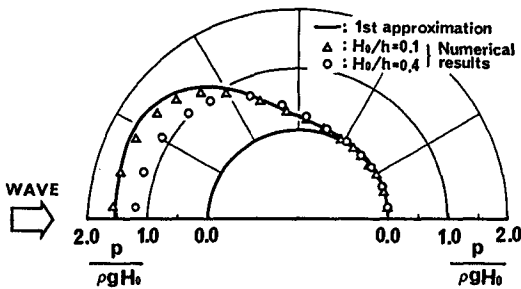
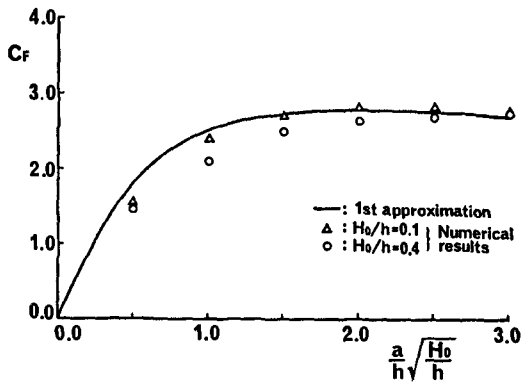
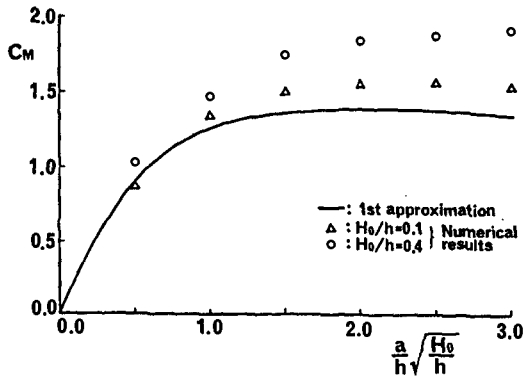


Fig. 8 Distribution of hydrodynamic pressure at  $z/h = -0.1$  when  $F_x$  is at the maximum with  $(a/h)\sqrt{H_0/h} = 2.0$ .



(a)  $C_F$



(b)  $C_M$

Fig. 9 Variations of  $C_F$  and  $C_M$  with  $(a/h)\sqrt{H_0/h}$ .

### 5. CONCLUSION

A numerical method has been developed for simulating solitary wave diffraction around large structures. The proposed method is based on the nonlinear potential theory, and it improves the time-stepping procedure of the conventional boundary element methods to provide greater accuracy. The effect of the improvement on the numerical solution has been shown by the simulation of a more realistic solitary wave profile.

Comparisons have been carried out with the first approximation for the horizontal

force and the overturning moment, acting on a circular cylinder. The first approximation gives reasonable results when  $H_0/h$  is about 0.1. When  $H_0/h = 0.4$ , however, the same approximation remarkably underestimates the overturning moment.

## REFERENCES

- Eatoock Taylor, R., and Hung, S. M., 1987: Second order diffraction forces on a vertical cylinder in regular waves, *Appl. Ocean Res.*, **9** (1), 19-30.
- Fenton, J.D., 1972: A ninth-order solution for the solitary wave, *J. Fluid Mech.*, **53**, 257-271.
- Hunt, J. N., and Baddour, R. E., 1981: The diffraction of nonlinear progressive waves by a vertical cylinder, *J. Mech. Appl. Math.*, **34**, 69-87.
- Isaacson, M de St Q., 1982: Nonlinear-wave effects on fixed and floating bodies, *J. Fluid Mech.*, **120**, 267-281.
- Isaacson, M de St Q., 1983: Solitary wave diffraction around large cylinder, *J. Waterway, Port, Coastal and Ocean Eng.*, ASCE, **109**, 121-127.
- Isaacson, M de St Q., and Zuo, Q.-H., 1989: Nonlinear wave forces on a circular cylinder, *Can. J. Civ. Eng.*, **16**, 182-187.
- Nakayama, T., and Washizu, K., 1981: Boundary element method applied to analysis of two-dimensional nonlinear sloshing problems, *Int. J. Numer. Methods Eng.*, **17**, 1631-1646.
- Ohyama, T., 1985: Boundary element analysis for solitary wave reflection and induced forces, *Proc. 32nd Japanese Conf. Coastal Eng.*, 555-559 (in Japanese).
- Ohyama, T., 1989 a: Boundary element analysis for run-up of nonlinear water wave, *Tech. Papers ISCFD-NAGOYA*, 377-382.
- Ohyama, T., 1989 b: A boundary element analysis for nonlinear wave diffraction around large structure, *Proc. JSCE*, **411**, 197-206 (in Japanese).